High-current space-charge-limited pulses using ultrashort laser pulses

Channprit Kaur,* Karumudi Rambabu, and Robert Fedosejevs
Department of Electrical and Computer Engineering, University of Alberta, Edmonton, Alberta, Canada

(Received 7 August 2022; accepted 10 October 2022; published 4 November 2022)

The maximum current that can be delivered by a 1-D vacuum diode is limited due to the space-charge reduction of the accelerating field. For a steady-state operation, this is given by the Child-Langmuir space-charge limit. However, for pulsed diode sources, the instantaneous current can be much higher than this limit, as long as the pulse length is much less than the transit time across the diode gap. This enables the generation of high current pulses with pulse durations of the order of tens of picoseconds using photocathodes driven by ultrashort laser pulses. The generation of such short and powerful electromagnetic pulses is important for numerous applications such as ultrawideband radar or as photocathode sources for accelerators. In this work, the limiting current pulse is investigated in the case of a very short, square-top initial pulse and it is found that these pulses propagate in a self-similar manner, remaining as a square-top charge cloud in space throughout their acceleration and propagation. The resultant current and pulse duration turn out to be dependent on only three parameters, which are the applied voltage, the vacuum transit time, and the fraction of the saturation charge density in the initial charge cloud. The resultant scaling of the resultant peak current and pulse duration are calculated numerically as a function of starting sheet-charge density, allowing the calculation of the resultant pulses for any ultrashort, pulse-driven vacuum photodiode design.

DOI: 10.1103/PhysRevE.106.055203

I. INTRODUCTION

The generation of short and powerful electromagnetic pulses (EMPs) is a major requirement for many applications such as ultrawideband (UWB) radar sensors. Such ultrashort electron bunches are also useful in generating picosecond x-ray pulses [1] in applications of ultrafast electron diffraction and microscopy [2,3] and as pulsed, high-brightness, picosecond electron guns for scanning electron microscopes [4]. Several techniques are employed for the design of conventional UWB pulse generators [5]. One technique for generating ultrashort electron pulses is to use a laser-driven photocathode excited by means of picosecond- or femtosecond-duration laser pulses. In this technique, the laser pulse generates an initial charge sheet cloud of electrons that are accelerated toward the anode under the application of an electric field. The peak current and minimum pulse duration that can be generated in such a system is limited by the space-charge spreading of the electron bunch and shielding of the applied field by the accelerating charge cloud, cutting off the acceleration of the trailing electrons. As already reported in previous publications [6,7], the peak current can significantly exceed the classical steady-state Child-Langmuir current limit [8] for such transient pulses with durations shorter than the diode gap transit time. In addition, a number of studies have focused on space charge effects on electron emission [9]. In these previous studies, approximate models giving estimates of the change in transit time and saturation currents are given. However, a complete description of the pulse duration and peak current versus charge-cloud areal density has not been given previously in the literature.

In this work, we derive the 1-D space-charge-limited transient current pulse for an instantaneous charge sheet slab generated by an ultrashort laser pulse from a photocathode. We demonstrate that for a flat-top charge sheet in the length direction, the pulse shape remains flat in space as it accelerates, and the acceleration and propagation of the pulse evolves in a self-similar manner. Such a self-similar response, which only depends on the scaled variables, is a well-known behavior for many partial differential equation problems [10]. This allows a prediction of the resultant peak current and pulse duration for any 1-D vacuum diode configuration. As a result, it is possible to design 1-D vacuum photo diodes driven with ultrashort laser pulses as an effective technique to generate high-voltage, ultrashort UWB pulses, which can be scaled to deliver pulses required for UWB radar applications.

One can first assess the maximum current density, which can be drawn for a planar vacuum diode. The Child-Langmuir law provides the maximum steady current that can be transported across such a planar diode gap [11]. The maximum current density derived by solving the steady-state 1D Poisson equation ($\frac{d^2\Phi}{dx^2} = -\frac{\rho}{\varepsilon_o}$) is

$$J_{CL} = \frac{4\sqrt{2}}{9}\varepsilon_O\sqrt{\frac{e}{m}}\frac{V_o^{3/2}}{d^2}, \tag{1}$$

where Φ is the electric potential, J_{CL} is the maximum steady current density, V_o is the diode voltage, d is the vacuum gap separation, ε_O is the permittivity of free space, m is the electron mass, and e is the elementary charge. Equation (1) holds for a zero transverse magnetic field, single-species

*channpri@ualberta.ca

charged particles with zero initial velocity, and nonrelativistic acceleration under the electrostatic approximation. Any deviation from these conditions, such as changing to cylinder or spherical geometries, relativistic acceleration, etc., will lead to modified current density limits [6,7].

In this work, we will examine the scaling of pulse duration in the case of simple planar gap acceleration for such transient short-pulse current sources. The boundary condition of Eq. (1) is $\Phi = 0$ at $x = 0$ (cathode) and $\Phi = V_o$ at $x = D$ (anode). Equation (1) is independent of material properties. Regardless of the cathode material or cathode temperature, Eq. (1) gives the bound imposed by Poisson's equation.

In the case of ultrashort laser pulse generation of electrons from the photocathode, the bunch length of electrons is much shorter than the anode–cathode gap. In this case the instantaneous current density can then be much higher than J_{CL} [12]. This can be estimated in terms of a simple capacitor model where the possible maximum charge in a planar gap is CV_o, where C is the capacitance of the starting vacuum gap. For a planar gap, the capacitance is $\varepsilon_o A/d$, where A is plate area. The limiting average current in the gap will be on the order of CV_o/T_G, where

$$T_G = [2\, d^2\, m_e/(e\, \Phi_0)]^{1/2}, \tag{2}$$

where T_G is the transit time of an electron across the vacuum gap under the applied electric field.

The limiting steady-state current can be converted to Eq. (1) after multiplying by numerical factor 8/9 [12]. For a pulse length $\tau \ll T_G$, the maximum current density allowed or critical current density, J_{critical}, can be given approximately by

$$J_{\text{critical}} = CV_o/\tau A \ = (8T_G/9\tau)\, J_{CL}, \tag{3}$$

which is much higher than the J_{CL}. If the current density exceeds the J_{critical}, the field at the cathode drops to zero and no further emission of electrons is possible. However, pulse spreading during transit will increase any short starting pulse width and will lead to a final pulse duration, which is larger and depends on the areal charge density present. To predict the final pulse duration, a model must be developed for the propagation of the charge density cloud across the diode gap and the resultant spreading.

Present day ultrashort lasers can produce starting photocathode charge clouds of femtosecond to picosecond durations, which is typically much shorter than the gap transit time. Thus, the limiting pulse duration is given almost entirely by the space charge spread of the short starting charge sheet as it propagates across the gap. This is the case that is analyzed next in both analytic calculations and particle-in-cell (PIC) modeling. It is found that the solution is self-similar, and scales with the vacuum transit time and fraction of space-charge-limited sheet charge. These models will allow the prediction of pulse duration for a given sheet-charge density generated at the photocathode surface for any diode voltage and gap.

The initial electron cloud is generated by a femtosecond-to picosecond-duration optical pulse hitting the photocathode surface. To generate large electron pulses, the efficiency of the photocathode is important in order to minimize the required laser pulse fluence. Different photocathodes made up of metals [1,8,13] and semiconductors can be used for this purpose. Despite the low quantum efficiency of metals, their high damage threshold, long lifetime, and ultrafast response often make them advantageous. Standard high-quantum-efficiency photocathode materials such as CsI, SbCs, and CsTe photocathodes can also be employed, but may suffer damage when very short high-current density pulses are extracted [14,15]. Thus, in order to obtain long-term stable operation, metal or semiconductor photocathodes may be required.

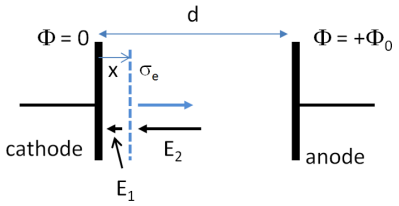

FIG. 1. Transient charge sheet inside a vacuum diode gap.

II. PICOSECOND PULSE MODEL

A number of authors have previously considered the short-pulse transient space-charge-limited diode response when driven by an optical pulse [7,12]. Two situations have been considered by past authors. The first is the limiting value of an instantaneous thin-sheet charge generated by the optical pulse at the photocathode. As shown in Fig. 1, this limiting value is given by a charge sheet whose electric field jump, E_2–$E_1 = E_0$, where $E_0 = \Phi_0/d$ is the electric field of the vacuum diode gap, with Φ_0 the anode potential and d the diode gap distance. Note that the electric fields are considered positive in the direction indicated. This leads to a zero electric extraction field on the cathode side of the charge sheet, cutting off extraction of further electrons from the cathode just as the charge sheet leaves the photocathode. We can define this limiting saturation sheet charge as

$$\sigma_{\text{sat}} = \varepsilon_0 \Phi_0/d. \tag{4}$$

This is equal to the areal charge density on the surface of the vacuum diode when one considers its capacitance given by

$$C = A\, \varepsilon_0/d, \tag{5}$$

where A and d are the area and plate separation respectively. The charge on a capacitor is given by $Q_C = \Phi C$, which leads to the plate charge per unit area of $Q_C/A = \varepsilon_0 \Phi_0/d$, the same as the saturation sheet charge density given by Eq. (4).

A second method of estimating the limiting sheet charge for transient charge sheets of duration τ has been given by Valfels *et al.* [12], where it is assumed that a Child-Langmuir limiting current distribution is established from the diode cathode toward the anode for the case of constant current-density injection of J_o over a pulse duration of τ. This solution assumes constant current injection over a period of time and does not account for subsequent space-charge spreading of the pulse as it then propagates across the gap to the anode.

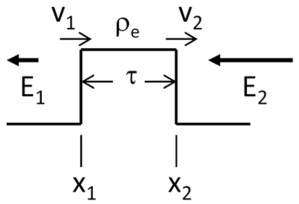

FIG. 2. Transient charge sheet in flight inside a vacuum diode gap, where the charge density is given by ρ_e (x). The positions of the front (2) and back (1) surfaces are given by x_2 and x_1, and the velocities by v_2 and v_1, respectively. The electric field on front of the charge sheet is E_2 and the electric field behind the charge sheet is E_1, with directions as indicated.

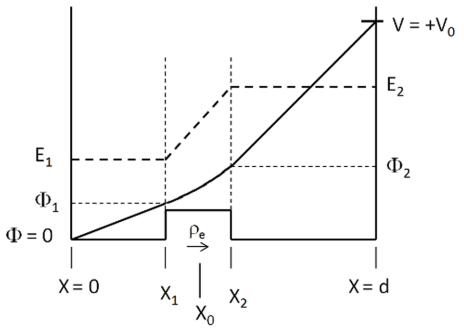

FIG. 3. Potential (solid line) and electric field (thick dashed line) distribution across the diode gap.

III. MODEL ASSUMPTIONS

In the present case, we are interested in calculating the exact pulse duration of the space-charge-limited pulses for a vacuum diode excited by a very short laser pulse of a duration of femtoseconds to picoseconds. We derive this model in classical limits for millimeter-range anode-cathode gaps and do not incorporate any quantum effects that generally arises in nanometer diode gaps [16,17]. We will not consider the transient emission process, but rather assume that a charge cloud of areal charge density σ has been produced by the optical pulse at a distance of a few microns from the cathode surface. For simplicity, we will assume that the charge cloud is flat topped in shape, as shown in Fig. 2. We will show in the end that a flat-top charge sheet accelerates in a self-similar manner and remains flat topped throughout its flight across the diode gap.

We now consider the equations of motion for acceleration of the leading and trailing edges of the charge sheet with the absolute value of the total areal charge density given by σ. The electrons at the leading and trailing edges of the charge sheet see electric fields of E_1 and E_2, respectively, and are accelerated according to the equation

$$dv_{1,2}/dt = E_{1,2}/m_e. \tag{6}$$

The electric fields on front and behind the charge sheet evolve in time as the flat-topped space charge cloud propagates across the gap from $x = 0$ to $x = d$. The jump in electric field across the total charge sheet remains constant, given by the absolute value of the integrated areal charge density according to

$$\Delta E = E_2 - E_1 = \sigma/\varepsilon_0. \tag{7}$$

The potential distribution across the diode gap also evolves in time, having linear slopes in the vacuum regions in front of and behind the space charge cloud, and a parabolic variation through the space charge cloud, as shown schematically in Fig. 3. The electric field is constant in the two vacuum regions in front of and behind the charge cloud, and has a linear dependence on position throughout the charge cloud due to the uniform flat-top charge distribution.

The self-consistent electric fields and potential distribution can be found for any position of the space charge cloud in the gap as follows. Consider the charge cloud in flight with positions of the leading edge X_2, the trailing edge X_1, and the thickness $\Delta X = X_2–X_1$. The midpoint of the charge cloud is given by $X_0 = (X_1 + X_2)/2$. The areal density is given by $\rho_e = \sigma/\Delta X$. The electric field in the region of X_1 to X_2 is given by Maxwell's equations as

$$dE(x)/dx = \rho_e/\varepsilon_0 = \sigma/(\varepsilon_0\,\Delta X) = \Delta E/\Delta X, \tag{8}$$

giving

$$E(x) = E_1 + \Delta E(X - X_1)/\Delta X, \quad (\text{for } X_1 < x < X_2). \tag{9}$$

Integrating this electric field from X_1 to X_2 gives the potential jump from Φ_1 to Φ_2, giving

$$\Phi_2 = \Phi_1 + (E_1 + \Delta E/2)\Delta X. \tag{10}$$

Using the relations $\Phi_1 = E_1\,X_1$ and $\Phi_2 = \Phi_0–E_2(d–X_2)$, one can write Eq. (9) in terms of electric fields and solve for E_1 and E_2, which are then given by

$$E_1 = E_0[1 - f_s\,(d - X_0)/X_0 \tag{11}$$

and

$$E_2 = E_0(1 + f_s\,X_0/d), \tag{12}$$

where f_s is the fractional charge saturation given by

$$f_s = \sigma/\sigma_{\text{sat}} = \Delta E/E_0 \tag{13}$$

and $E_o = \Phi_0/d$. The acceleration of the two end points, X_1 and X_2, can now be calculated using the fields at the two ends of the charge cloud, E_1 and E_2. The equations of motion for the two end points can then be integrated numerically in time to give the trajectories of the two end points of the charge slab and the resultant spread in time of the charge cloud. This can be carried out numerically, noting that X_0 is given at each time step as the average of X_1 and X_2.

A. Self-similar behavior of current pulse

In order to show that the flat-top charge distribution remains flat top, one can use the 1D divergence equation relating time rate of change of density to divergence in the particle flux given by

$$d\rho_e/dt = -d(\rho_e v)/dx. \tag{14}$$

Assuming that $\rho_e(x)$ is a constant in x over the charge region, then the time rate of change in $\rho_e(x)$ is given by

$$d\rho_e/dt = -\rho_e dv/dx \quad (\text{for } X_1 < x < X_2). \tag{15}$$

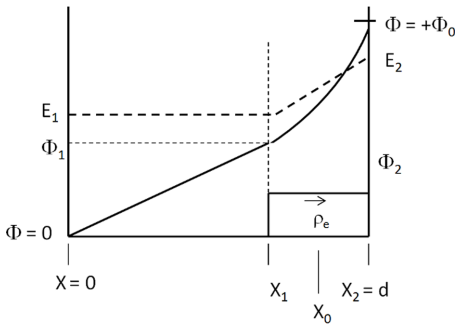

FIG. 4. Potential (solid line) and electric field (thick dashed line) distribution across the diode gap as the charge is being absorbed on the positive anode.

The velocity distribution is given from the acceleration of the charge species from $t = 0$, starting at rest. The acceleration, in turn, is given by the electric field at each point in the slab, which varies linearly from X_1 to X_2, giving an acceleration varying linearly in position from X_1 to X_2 given

$$a(x,\, t) = a_1(x,\, t) + \Delta a\,(x - X_1)/\Delta X \quad (\text{for}\, X_1 < x < X_2), \tag{16}$$

where

$$\Delta a = e\,\Delta E/m \quad (\text{for} \quad X_1 < x < X_2), \tag{17}$$

and e is the fundamental unit of charge and m_e is the mass of an electron. Note that Δa is a constant in time dependent on the initial areal charge-sheet density, just as ΔE is a constant in time. We can integrate Eq. (16) starting from zero velocity at $t = 0$ for all positions in the charge slab, giving the velocity

$$v(x,\, t) = v_1(x,\, t) + \Delta a\, t\,(x - X_1)/\Delta X \quad (\text{for}\, X_1 < x < X_2). \tag{18}$$

We can now evaluate the derivative of velocity with respect to x by differentiating Eq. (18), giving

$$dv/dx = \Delta a\, t/\Delta X \quad (\text{for}\, X_1 < x < X_2). \tag{19}$$

This shows that dv/dx is a constant in space at any instant in time, resulting in $d\rho_e/dt$ being uniform in space over the whole charge slab at any instant in time. Thus, every point in the charge slab decreases in density at the same rate in time, resulting in a uniform charge slab decreasing uniformly in density in time. This results in the density profile remaining flat topped at every instant in time.

Indeed, one can show that the solution is self-similar, with the self-similar scaling parameters given by the time of flight for an electron across the vacuum gap, $T_G = [2\mathrm{d}^2\, m_e/(e\,\Phi_0)]^{1/2}$, and the saturation fraction of the charge density, f_s. Thus, the solution for the spread in the pulse for any case can be calculated in terms of these two parameters.

A final correction is required as the pulse is absorbed on the anode plate. The situation changes as shown in Fig. 4, where only part of the charge remains in the gap. In this case the charge σ is decreasing in time and the shielding effect starts to decrease. However, at every instant in time, the situation is identical to the initial solution, with a reducing charge in time within the gap. The previous distribution of electric field and potentials can be used with the reduced remaining charge. The arguments leading to the flat-top charge distribution remaining as a flat top are still valid, and thus the rectangular shape of the charge slab in space always remains rectangular still. This then leads to a self-similar solution that also scales with the vacuum transit time T_G and the ratio of the initial charge-sheet areal density to the saturation charge-sheet areal density f_S, because the arrival velocity of the charges decreases with time throughout the pulse. The actual temporal pulse shape observed on the anode decreases in time with a characteristic shape given by the ratio of starting charge to saturation charge f_S.

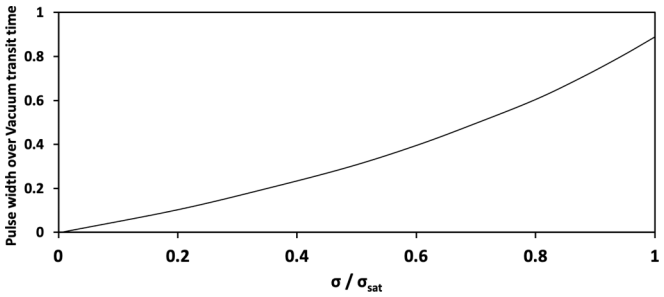

FIG. 5. Output pulse width versus slab charge scaled to the vacuum transit time and the saturation charge areal density, respectively.

Based on the electric field at the front and back of the charge sheet as given by Eqs. (11) and (12), the trajectories of the front, X_2, and back, X_1, of the charge slab have been calculated numerically using a fourth-order Runge–Kutta solver to an accuracy of better than 10^{-3}. The corrections as the pulse is absorbed into the anode are also included to give the complete temporal profile of the pulse. The initial charge sheet is positioned between 1 and 2 microns from the cathode surface in these numerical calculations, for a diode gap of 3 mm. The ratio of output pulse width, $\Delta\tau$, to the vacuum transit time, T_G, is plotted in Fig. 5 as a function of the ratio of slab charge to saturation charge density. The pulse width refers to the total time from the start to the end of the pulse arriving at the anode, i.e., from the arrival of the first electron in the pulse to the last electron in the pulse. In order to compare to a real physical system, the pulse widths are calculated for the case of a 3 mm diode gap, with various potentials ranging from 1 kV to 5 kV applied to the anode. The resultant pulse widths are plotted in Fig. 6. The resultant response curve can be fit by a

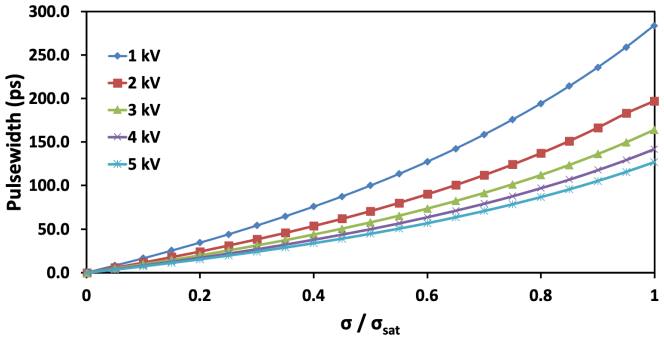

FIG. 6. Output full-pulse width versus fractional charge slab charge for a 3-mm-gap vacuum diode.

TABLE I. Coefficients for the fourth-order polynomial fit for the self-similar pulse width versus charge density as shown in Fig. 5, $\Delta\tau/T_G = \sum a_i \times (\sigma/\sigma_{sat})^i$, where $\Delta\tau = \tau_1 - \tau_2$, self-similar arrival time of the leading edge of the pulse $\tau_1 = t_1/T_G = \sum b_i \times (\sigma/\sigma_{sat})^i$, and self-similar end time of the pulse $\tau_2 = t_2/T_G = \sum c_i \times (\sigma/\sigma_{sat})^i$.

$i=$	0	1	2	3	4
a_i	0.0000	0.4882	0.2582	–0.0853	0.2387
b_i	1.0000	–0.0821	0.0541	–0.0135	0.0028
c_i	1.0000	0.4061	0.3123	–0.0988	0.2415

fourth-order polynomial using the coefficients listed in Table I to an accuracy on the order of 0.1%.

The output current-density pulse shape is also a self-similar function of the saturation parameter f_s, the self-similar scale current density given by $J_{ss} = \sigma_{sat}/T_G$ and the scaled time $\tau_{ss} = t/T_G$. Representative examples of the output current-density pulse shape, i.e., time rate of change of charge entering the anode, for various ratios of charge density to the saturation charge density are given in Fig. 7(a) for the case of $V_0 = 3$ kV and $d = 3$ mm. The self-similar pulse shape in terms of the J_{ss} and τ_{ss} is plotted in Fig. 7(b).

It can be seen that even though the pulse is flat topped in space at all times as it propagates in the diode gap (even as it is entering the anode), the pulse drops in time due to the continuous spreading of the pulse in time as it propagates and due to the reduction in space-charge shielding as the electrons are absorbed at the anode.

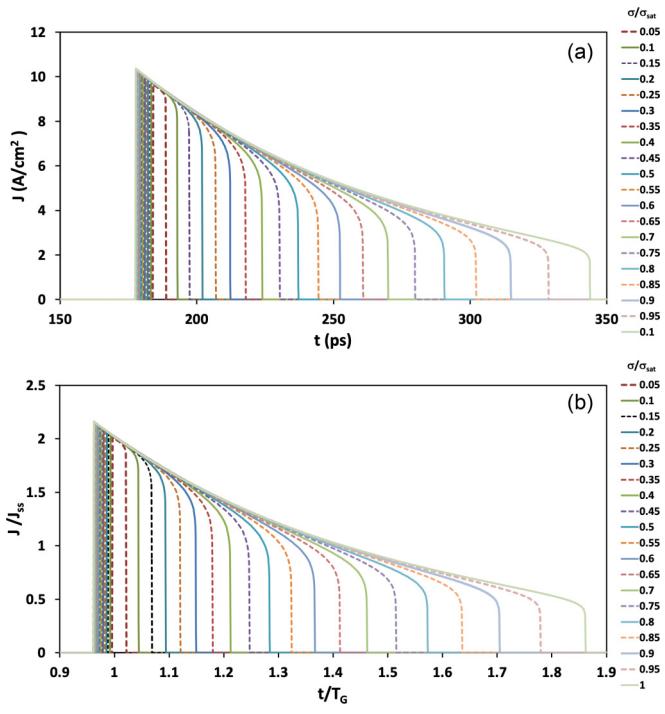

FIG. 7. Output pulse shapes for a 1 cm^2 diode with a 3 mm gap and a 3 kV gap potential (a) for various values of σ/σ_{sat} and (b) the self-similar pulse shape in terms of the self-similar current density J_{ss} and scaled time.

TABLE II. Coefficients for the functional fit for the self-similar current density pulse shape versus normalized time as shown in Fig. 7 for decimal values of the normalized charge density. $J_{ss}(\tau) = d_{k0} + d_{k1} \times \tau + d_{k2} \times \tau^2 + d_{k3} \times \tau^3 + d_{k4} \times \tau^4$ for starting charge density fraction $f_s = k/10$.

$i=$	0	1	2	3	4
d_{1i}	2.0354	–2.6206	–68.834	2572.4	–40149
d_{2i}	2.0598	–2.8444	–25.273	480.31	–3648.9
d_{3i}	2.083	–3.0581	–10.764	145.64	–720.28
d_{4i}	2.1033	–3.216	–4.9323	59.269	–210.45
d_{5i}	2.1206	–3.3703	–1.437	24.905	–69.421
d_{6i}	2.1352	–3.5105	–0.7265	9.9558	–23.933
d_{7i}	2.1463	–3.6308	2.0763	3.2031	–8.1603
d_{8i}	2.1555	–3.7358	2.9504	0.0048	–2.399
d_{9i}	2.1613	–3.822	3.5144	–1.5198	–0.2823
d_{10i}	2.1659	–3.8938	3.8685	–2.2123	0.4528

B. Scaling law for temporal pulse profiles

In order to provide a simple way of calculating the temporal response of the diode for any saturation value, a least-squares fourth-order polynomial fit is carried out to the self-similar current density, $J_{ss}(\tau)$, as a function of the self-similar time variable $\tau = (t/T_G) - \tau_{str}$, where τ_{str} is the arrival time of the first electron. This is carried out for decimal values of the normalized charge densities, f_s,

$$J_{ss}(\tau) = d_{k0} + d_{k1} \times \tau + d_{k2} \times \tau^2 + d_{k3} \times \tau^3 + d_{k4} \times \tau^4, \tag{20}$$

where $k = 10 \times f_s$, the scaled fractional charge density. Each fit starts at $\tau = 0$, corresponding to τ_{str}, and ends at $(\tau_{end} - \tau_{str})$ for each value of normalized charge distribution f_s. The fits are carried out over the first 90% of the pulse duration and are not fit to the falling end of the pulse. The coefficients for these fits are given in Table II. The accuracy of the fits is better within 0.4% in the first 90% of the pulse length. There is a small discrepancy at the end of the pulse, where the model calculation shows a drop in the pulse as it is absorbed into the anode, which is not modeled with the curve fit here. In reality, the detailed shape of the pulse once it starts to enter the anode will be affected by the circuit parameters of the anode and subsequent flow of current down the transmission line used to extract the current pulse, which are not modeled here. However, these fits should prove useful in modeling the shape of the pulse generated over a variety of parameters.

A few calculated fits using the parameters from Table II are compared to the numerical calculated profiles in Fig. 8.

IV. PARTICLE-IN-CELL MODELING

In order to verify the self-similar analytic solutions derived earlier, numerical modeling of the transient pulse generation was carried out using a 1D nonrelativistic electrostatic PIC code [18]. This was used to predict the expected pulse shapes as a function of electron charge created through the space-charge-limit regime. The electrons are mobile along the x direction. The electric field is directed along the x-axis. A total of 3000 mesh points were chosen along the x-axis, with each mesh point equal to 1 μm. The cathode is located at

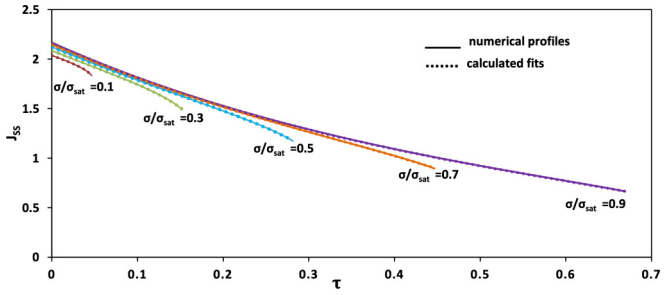

FIG. 8. Output self-similar pulse shape in terms of the self-similar current density J_{ss} and time τ from the start of the pulse for a few fixed saturation fluxes. The numerical profiles are plotted as solid lines and the calculated fits as dashed curves.

$x = 0$ with zero potential, and the anode is at $x = 3$ mm with finite potential. The electron areal number density varies from 1.8×10^8 to $7 \times 10^9/\text{cm}^2$, and potential from 1.2 kV to 5 kV is varied for different cases to explore the current-density limitation. The number of macroparticles used was 50 000. At the initial time, all the particles are located at the 1 μm position from the cathode surface, with the pulse width equal to zero. The electrons have no initial velocity. The time-dependent profile of potential, electric field, and positions for electrons are written after every 40 fs. Figure 9 shows the spatial profile of electrons for a 3 kV potential and 4.95×10^9 cm^{-2} areal number density ($\sigma/\sigma_{\text{sat}} = 0.9$) at 175 ps [Fig. 9(a)] and a temporal profile reaching at the anode [Fig. 9(b)]. It is seen that indeed the pulse shape remains flat topped in space as it propagates and, as expected, the current observed on the anode decreases in time as the pulse arrives. The sharp spikes observed at the start and end of the PIC simulation pulses are

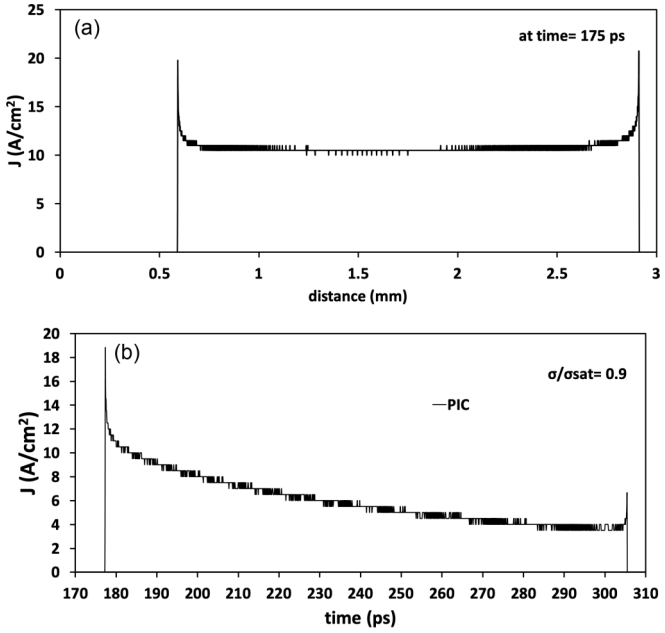

FIG. 9. Particle-in-cell simulation results: (a) spatial profile of electrons in flight at 175 ps and (b) temporal profile of the electron pulse at the anode, for a 3 kV potential across the electrodes and 4.95×10^9 cm^{-2} areal number density of electrons ($\sigma/\sigma_{\text{sat}} = 0.9$).

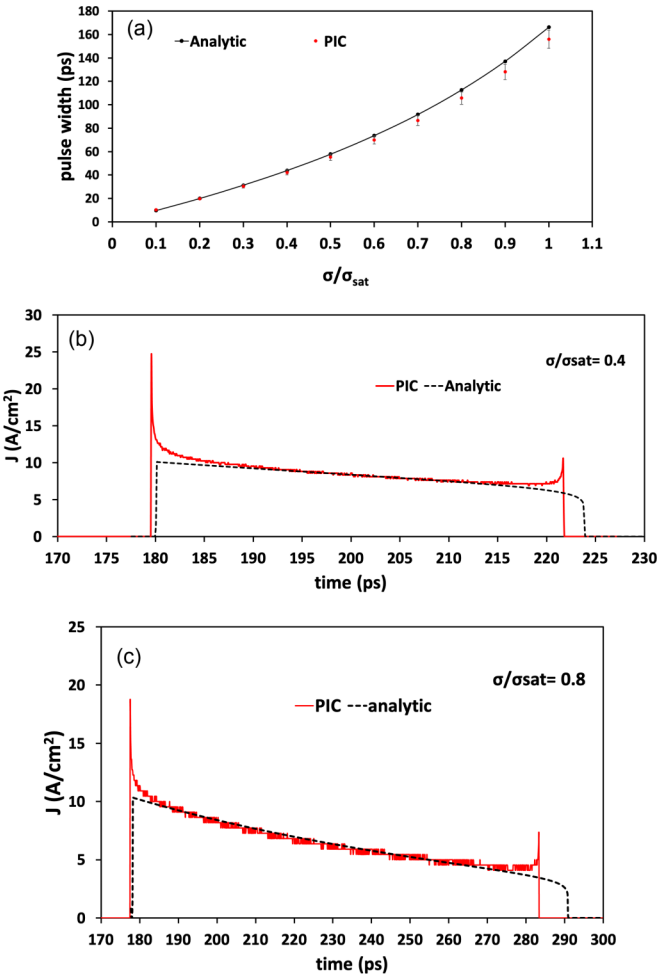

FIG. 10. (a) Calculated full pulse width arriving at the anode versus the fractional charge slab density for a 3 mm gap and a 3 kV potential vacuum diode. Data for both the analytic solution and the PIC simulations are shown. Pulse profiles for both PIC simulations and the analytic solution are shown in (b) for $\sigma/\sigma_{\text{sat}} = 0.8$ and (c) for $\sigma/\sigma_{\text{sat}} = 0.4$.

artifacts of the numerical solver routines at the sharp edges of the pulse.

A. Comparison of analytic and PIC results

The full output pulse widths calculated by the self-similar model and calculated from the PIC simulations are compared in Fig. 10 for the case of a potential of 3 kV and a gap of 3 mm. In fact, the actual pulse shape will be nonuniform in time, as shown in Fig. 7(b).

V. GENERATION OF 100 ps PULSES INTO A 50 Ω LOAD

One of the applications of diode-driven ultrashort pulses is for the excitation of 100 ps broadband pulses for millimeter imaging radar. To assess the potential scaling of such a source, the case of a practical diode with a 3 mm gap and various anode potentials is used as a practical example case. It is assumed that the photocathode is driven by an ultrashort femtosecond-to-picosecond-duration laser pulse. For

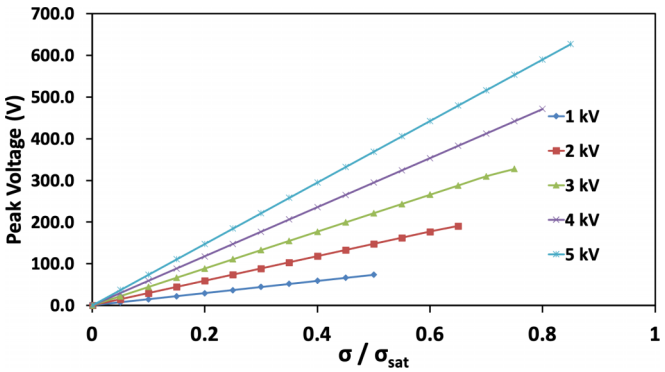

FIG. 11. Predicted peak output voltage in a simple 100-ps square-top shape after pulse shaping of the output versus the fractional charge slab charge for a 3-mm-gap vacuum diode for a 1 cm^2 photocathode area. Curves are plotted for each potential up to the point where the pulse width exceeds 100 ps.

simplicity it is assumed that the photodiode is attached to a pulse shaper and transmission line in order to form a 100 ps output pulse. The peak voltage that can be generated is given by the total charge times 50 Ω divided by the assumed 100 ps output pulse width, and is plotted in Fig. 11 versus the diode potential up to the point where the actual diode output pulse duration would exceed 100 ps. Thus, the peak voltage represents the expected voltage that could be achieved assuming a simple square-top pulse. It is seen that output pulses with a peak of several hundred volts can be produced for a 1 cm^2-area diode, which would be of great practical importance for the excitation of millimeter radar imaging systems. In reality, the pulse would have a more complex pulse shape, depending on the details of the subsequent transmission line and output circuit, but this estimate should give a good indication of the peak voltages achievable.

In order to excite such pulses, either high-efficiency photocathodes based on low work-function cathode materials excited by visible pulses or simple metallic photocathodes excited by UV laser pulses can be employed. For example, to produce a 500 V pulse into 50 Ω in a 100 ps pulse duration requires a charge of 1 nC. Using a standard bialkali visible photocathode with a responsivity of around 50 mA/W would require a laser pulse of 20 nJ energy. However, the instantaneous current density in such a photocathode may lead to damage, and thus the maximum voltages that can be achieved in practical systems with standard low work-function photocathodes will probably be less than this. In principle, larger output voltages can also be achieved by using larger photocathode areas, but this is also limited by the larger effective pulse widths given by the extended spatial size of the source, where the propagation distance across the source region is limited by the speed of light to be less than 3 cm to achieve a pulsewidth of less than 100 ps. The use of high-damage-threshold metallic photocathodes would allow operation up to the values calculated here. However, in this case, UV pulses of around 260 nm or less in wavelength are required for excitation, and the photocathode quantum efficiencies are on the order of 10^{-3} at best [19]. Using fourth harmonic output from a 1 μm laser would require an energy per pulse at the fourth harmonic of approximately 5 μJ of laser energy per pulse. Assuming a 10% conversion efficiency from the fundamental to the fourth-harmonic wavelength in the laser would require a laser with a pulse energy of 50 μJ per pulse at the fundamental wavelength. Given the availability of picosecond laser systems with output power on the order of 1 W, one has the potential of generating 500 V, 100 ps electrical pulses at a rate of 50 MHz if bialkali photocathodes can be employed, or at 20 kHz using high-damage-threshold metallic photocathodes.

VI. CONCLUSION

We have developed a self-similar analytic model to assess quantitatively the generation of short EMPs using planar vacuum photodiodes excited by ultrashort laser pulses. The output pulse width, peak current, and pulse shape are given by the model in terms of two scaling parameters—namely, the vacuum transit time and the ratio of areal charge density relative to the space charge saturation charge density. With these parameters, one can predict the output of any planar vacuum diode excited by an ultrashort laser pulse. These pulse shapes can then be used as input pulses to the transmission line, pulse shaping, and antenna circuits for the launching of millimeter wave pulses for imaging applications.

The results indicate that by employing large applied potentials, large-area photocathodes, and sufficient pulse energy, electron pulses with a duration of 100 ps or less can be generated into 50 Ω loads, achieving peak output voltages of several hundred volts per pulse. In addition, the use of high-efficiency photocathode materials would allow the generation of such pulses with repetition rates above 1 MHz with currently available laser sources. Such sources would be of interest for applications such as millimeter wave imaging.

ACKNOWLEDGMENTS

This research was supported by the Natural Sciences and Engineering Research Council of Canada Research Grant No. RGPIN-2019-05013.

[1] B. Van Wonterghem and P. M. Rentzepis, Appl. Phys. Lett. **56**, 1005 (1990).
[2] Z. Tao, H. Zhang, P. M. Duxbury, M. Berz, and C.- Y. Ruan, J. Appl. Phys. **111**, 044316 (2012).
[3] D. A. Plemmons and D. J. Flannigan, Chem. Phys. Lett. **683**, 186 (2017).
[4] M. Merano, S. Collin, P. Renucci, M. Gatri, S. Sonderegger, A. Crottini, J. D. Ganière, and B. Deveaud, Rev. Sci. Instrum. **76**, 085108 (2005).
[5] R. S. C. Winter, D. Oloumi, and K. Rambabu, IEEE Trans. Microw. Theory Tech. **69**, 297 (2021).
[6] A. D. Greenwood, J. F. Hammond, P. Zhang, and Y. Y. Lau, Phys. Plasmas **23**, 072101 (2016).

[7] P. Zhang, A. Valfells, L. K. Ang, J. W. Luginsland, and Y. Y. Lau, Appl. Phys. Rev. **4**, 011304 (2017).
[8] T. Anderson, I. V. Tomov, and P. M. Rentzepis, J. Appl. Phys. **71**, 5161 (1992).
[9] K. L. Jensen, J. Lebowitz, Y. Y. Lau, and J. Luginsland, J. Appl. Phys. **111**, 054917 (2012).
[10] G. I. Barenblatt, *Similarity, Self-similarity, and Intermediate Asymptotics* (Consultants Bureau, New York, 1979).
[11] C. D. Child, Phys. Rev. (Series I) **32**, 492 (1911).
[12] A. Valfells, D. W. Feldman, M. Virgo, P. G. O'shea, and Y. Y. Lau, Phys. Plasmas **9**, 2377 (2002).
[13] J. Smedley, T. Rao, and Q. Zhao, J. Appl. Phys **98**, 043111 (2005).
[14] S. H. Kong, J. Kinross-Wright, D. C. Nguyen, and R. L. Sheffield, Nucl. Instrum. Methods Phys. Res. A Accel. Spectrom. Detect. Assoc. Equip. **358**, 272 (1995).
[15] B. L. Henke, J. P. Knauer, and K. Premaratne, J. Appl. Phys. **52**, 1509 (1981).
[16] L. K. Ang and P. Zhang, Phys. Rev. Lett. **98**, 164802 (2007).
[17] P. Zhang, Y. S. Ang, A. L. Garner, A. Valfells, J. W. Luginsland, and L. K. Ang, J. Appl. Phys. **129**, 100902 (2021).
[18] K. Patel, https://github.com/letapk/espic1d (2015).
[19] Hamamatsu Photonics K. K. *Photomultiplier Tubes: Basics and Applications*, 3rd ed. (2007).